Advanced Composite Materials
Publication details, including instructions for authors and subscription information:
http://www.tandfonline.com/loi/tacm20

Modeling of thermo-mechanical behavior of Ti-Ni shape memory alloy foils embedded in carbon fiber reinforced plastic laminates

Ichiro Taketa , Masataro Amano , Masakazu Kobayashi , Toshimichi Ogisu , Yoji Okabe & Nobuo Takeda
Version of record first published: 02 Apr 2012.

To cite this article: Ichiro Taketa , Masataro Amano , Masakazu Kobayashi , Toshimichi Ogisu , Yoji Okabe & Nobuo Takeda (2005): Modeling of thermo-mechanical behavior of Ti-Ni shape memory alloy foils embedded in carbon fiber reinforced plastic laminates, Advanced Composite Materials, 14:1, 25-42

To link to this article: http://dx.doi.org/10.1163/1568551053297111

Adv. Composite Mater., Vol. 14, No. 1, pp. 25–42 (2005)

Also available online - www.vsppub.com

Modeling of thermo-mechanical behavior of Ti-Ni shape memory alloy foils embedded in carbon fiber reinforced plastic laminates

ICHIRO TAKETA [1], MASATARO AMANO [1,*], MASAKAZU KOBAYASHI [1], TOSHIMICHI OGISU [2], YOJI OKABE [1] and NOBUO TAKEDA [1]

[1] *Takeda Laboratory, Department of Advanced Energy, Graduate School of Frontier Sciences, The University of Tokyo, 5-1-5, Kashiwanoha, Kashiwa-shi, Chiba, 277-8562, Japan*
[2] *Material Research Section, Research and Laboratory Department, Engineering and Development Center, Aerospace Company, Fuji Heavy Industries Ltd., 1-1-11, Yonan, Utsunomiya, Tochigi, 320-8564, Japan*

Received 8 April 2004; accepted 30 August 2004

Abstract—Ti-Ni shape memory alloy (SMA) foils are embedded into carbon fiber reinforced plastic (CFRP) cross-ply laminates in order to suppress the occurrence and progress of the transverse cracks in the laminates. When the pre-strained SMA foil is heated, the shape memory effect produces appropriate recovery compressive stress in the direction to suppress transverse cracks. However, Ti-Ni SMA foil has these specific characteristics due to the existence of a rhombohedral phase (R-phase). Thus, in this research, in order to use this SMA foil as an actuator, an extended Brinson model was proposed to clarify complicated behaviors of SMA. Then, for the determination of the parameters in the constitutive equation in this model, experimental tests were performed for the SMA foils. Using this model, several simulations were conducted and compared with experimental results. The agreement indicated that this model could express the thermo-mechanical behavior of the Ti-Ni SMA foil adequately. Finally, the behavior of the SMA foil during the CFRP manufacturing process was calculated on the basis of this model. The calculation results proved that the recovery stress already existed after the manufacturing process and the embedment of 4% pre-strained SMA into CFRP cross-ply laminate had the effect of suppressing the occurrence of transverse cracks.

Keywords: Shape memory alloys; composites; R-phase; extended Brinson model.

1. INTRODUCTION

While CFRP composites have high specific strength and specific modulus, complicated microscopic damage, such as transverse cracks, occurs inside the composite

*To whom correspondence should be addressed. E-mail: masa@smart.k.u-tokyo.ac.jp

laminates. Hence the application of CFRP to primary structural materials has been restricted. In order to extend the use of CFRP for further applications, it is necessary to clarify the fracture mechanisms and, furthermore, to produce smart composites that can suppress the damage occurrence and progress in the laminates. Considering these backgrounds, the authors have attempted to use a Ti-Ni SMA foil as an actuator to suppress the occurrence of transverse cracks in CFRP laminates.

SMA has shape memory effects that can fully recover its shape from the large residual (apparently plastic) strain by heating. This effect is due to solid state transformations between martensitic phase and austenitic phase, and it generates a large stress. Taking advantage of this effect, the SMA can be used as an actuator. Thus, the authors embed SMA foil into a CFRP laminate after a large residual strain (pre-strain) is applied to the SMA foil at room temperature. When the SMA foil is heated, the shape memory effect produces a recovery compressive stress along the longitudinal direction, so that it suppresses the occurrence and progress of transverse cracks as shown in Fig. 1. Ogihara *et al.* [1] reported experimentally that embedment of SMA fibers into composite laminate was effective in suppressing the damage occurrence and progress. However, the estimated damage suppression effect of SMA was small because of the small volume fraction of SMA fibers in the composite laminate. On the other hand, SMA foils have comparatively larger volume fraction in the laminate than SMA fibers. The authors reported

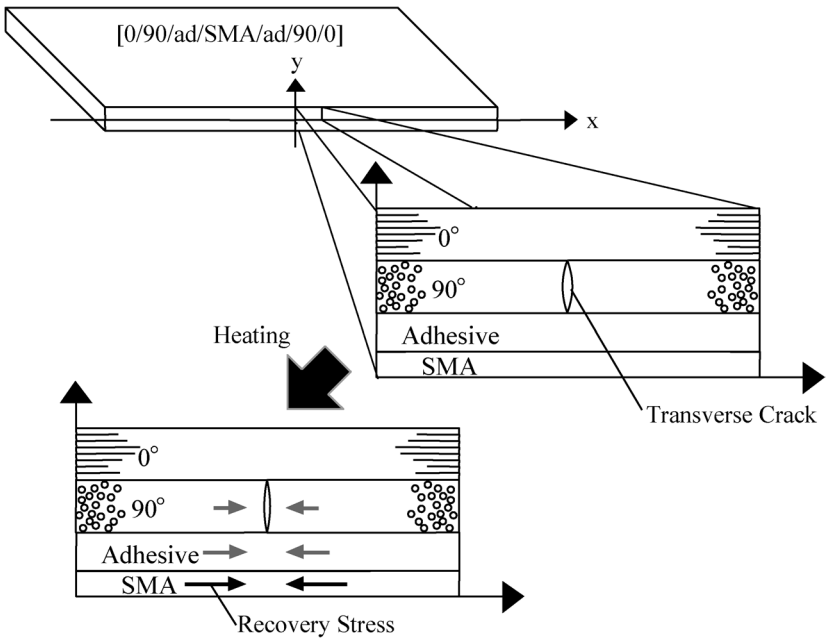

Figure 1. Mechanism that the recovery stress of an embedded SMA foil suppresses the occurrence of transverse cracks in a CFRP cross-ply laminate.

experimentally that SMA foils are expected to produce larger recovery force than SMA fibers [2].

Many constitutive models have been developed to describe the thermo-mechanical behavior of SMA. Tanaka [3] suggested one of the most popular one-dimensional models based on thermo-mechanics. In this model, the second law of thermodynamics was written in terms of the Helmholtz free energy. It was assumed that just three variables — uni-axial strain, temperature, and martensite volume fraction ξ — were the only state variables in this model. Volume fraction ξ was expressed in terms of stress and temperature. Then, Liang and Rogers [4] presented a model based on the constitutive equation developed by Tanaka. In their model, a cosine representation was used to describe the martensite volume fraction. However, these two models could describe only the stress-induced martensite transformation and did not consider temperature-induced martensite transformation. To overcome this deficiency, Brinson [5] developed a constitutive model that separated out the martensite volume fraction into two parts: martensite that was stress-induced and that which was temperature-induced. In this model, the coefficients of the constitutive equation were assumed to be non-constants.

In this research, Ti-Ni SMA foil was considered because it has high resistivity, good fatigue resistance, corrosion resistance and large reproducible shape recovery after temperature cycling. However, it has a third phase called the R-phase [6]. Since the R-phase has a rhombohedral structure and its transformation precedes the martensitic transformation, its behavior is different from the other SMA.

Some constitutive models including the effect of R-phase are developed. For example, Kamita and Matsuzaki proposed a phenomenological approach based on an energy consideration [7]. Though their approach well represented the behavior of Ti-Ni SMA foil, it is difficult to introduce it into some mechanical analyses and to analyze the effect of Ti-Ni SMA foil as an actuator. In order to use Ti-Ni SMA foil as an actuator, an extended Brinson model was newly proposed to clarify the complicated behavior. Then, parameters of this model were determined by several experiments. Finally, the behavior of the SMA foil was calculated analytically.

2. CONSTITUTIVE EQUATION OF SMA

In order to simulate the stress profile of the CFRP laminate with an embedded SMA foil, a comprehensive model to represent the behavior of SMA is required. In this section, after theoretical backgrounds are reviewed, an extended Brinson model is newly suggested.

2.1. Theoretical backgrounds

Generally, SMA consists of two phases: martensitic phase and austenitic phase. Thermo-mechanical loads cause a solid state transformation between the two phases. The transformation from austenite to martensite is known as martensitic

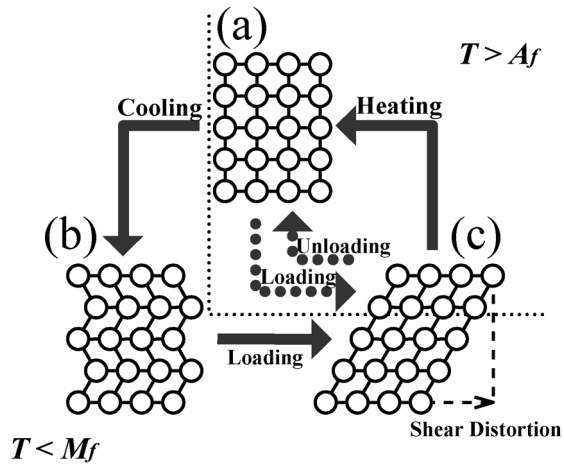

Figure 2. Schematic of shape memory effect and pseudoelasticity that are caused by de-twinning and phase transformation among (a) austenite, (b) twinned martensite, and (c) de-twinned martensite.

transformation, and that from martensite to austenite is called the reverse transformation.

Figure 2 shows the schematic of shape memory effect (SME) and pseudoelasticity of SMA. The SME is explained as follows. In Fig. 2, the phase (a) is the austenitic phase, and the phases (b) and (c) are the martensitic phase. M_f and A_f represent the transition temperatures: martensite finish and austenite finish, respectively. When SMA is cooled to less than M_f, multiple variants and twins appear, which are all crystallographically equivalent but which have different orientations (different habit plane indices). This transformation is called temperature-induced transformation from austenite (a) to martensite (b). At $T < M_f$, when a load applied to the phase (b) reaches a certain critical stress, the pairs of martensite twins begin 'de-twinning' to the stress-preferred twins. As a result, the multiple martensite variants (b) convert to the phase (c) according to the loading direction. Meanwhile, when the phase (c) is heated above the A_f, it transforms to austenite (a) again and recovers its original geometric configuration. This is called SME. Similarly, at $T > A_f$, when stress is applied to the phase (a), the austenite transforms to stress-induced martensite (c). But when the phase (c) is unloaded, it returns to the austenite (a) along a characteristic hysteresis loop, and the shape is recovered completely. This is called pseudo-elasticity [5].

In 1986, Tanaka [3] derived the constitutive equation of SMA from basic thermomechanical theory, which includes only state variables and material constants that can be measured experimentally. The constitutive equations are represented as

$$\mathrm{d}\sigma = D(\varepsilon, \xi, T)\,\mathrm{d}\varepsilon + \Omega(\varepsilon, \xi, T)\,\mathrm{d}\xi + \Theta(\varepsilon, \xi, T)\,\mathrm{d}T, \tag{1}$$

$$\Omega = -\varepsilon_L D(\varepsilon, \xi, T), \tag{2}$$

$$\Theta = -\alpha D(\varepsilon, \xi, T), \tag{3}$$

$$\xi = \Xi(\sigma, T), \tag{4}$$

where ε, ξ and T represent Green strain, martensite volume fraction and temperature respectively, and α is the thermal expansion coefficient. The martensite volume fraction ξ is defined as the martensite fraction of the material, which varies from 0 to 1. Stiffness tensor D, transformation tensor Ω and thermo-elastic tensor Θ are the functions of ε, ξ and T. The second Piola–Kirchoff stress tensor σ is calculated through the integral of the constitutive equation. The maximum residual strain (recovery strain limit) ε_L is the residual strain that can be achieved by converting austenite to completely de-twinned martensite by loading at the temperature where the reverse transformation does not occur.

In 1993, Brinson extended the martensite fraction ξ to the sum of purely temperature-induced martensite fraction ξ_T and stress-induced martensite fraction ξ_S [5].

$$\xi = \xi_S + \xi_T. \tag{5}$$

2.2. Extended Brinson model

The SMA used in this research is Ti-Ni alloy. This material has a third phase in addition to martensite and austenite, which is called the rhombohedral phase (R-phase) [6]. The R-phase can transform reversibly without hysteresis. This transformation precedes the martensitic transformation on tensile loading. In order to incorporate the R-phase into the constitutive equation, the authors propose a newly extended Brinson model.

In Fig. 3, the regions (1) and (2) show the martensite transformation and the reverse transformation respectively, and the regions (3) and (4) show the transformation from austenitic phase to R-phase and that from R-phase to austenitic phase respectively. The region (5) represents accommodation of R-phase, which is different from transformation. The authors incorporate all these regions into this model. In this material, the region (3) and the region (4) are considered to be the same because hysteresis does not appear in these transformations. The martensite transformation in the region (1) includes both the transformation from R-phase to martensitic phase and that from austenitic phase to martensitic phase. In this research, the stress coefficients C_M and C_A are assumed to be the same value, which are material properties that describe the relationship between temperature and the critical stress to induce transformation.

Martensite fraction ξ^M and R-phase fraction ξ^R are defined as the sum of the stress-induced fraction and the purely temperature-induced fraction as

$$\xi = \xi^M + \xi^R, \tag{6}$$

$$\xi^M = \xi_S^M + \xi_T^M, \tag{7}$$

$$\xi^R = \xi_S^R + \xi_T^R. \tag{8}$$

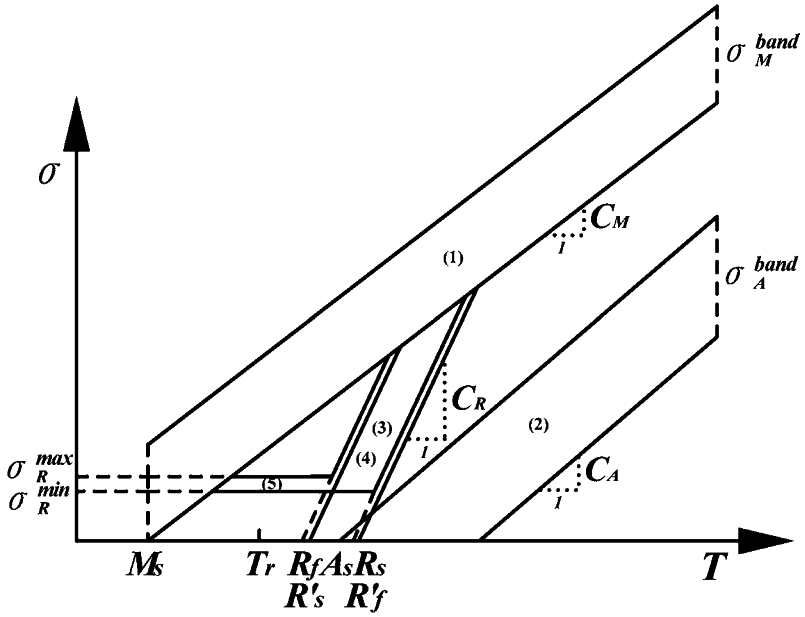

Figure 3. Critical stresses *versus* temperature representing transformations of Ti-Ni SMA. C_M and C_A are the slopes of the $\sigma_{crit}(T)$ curves for the austenitic phase to martensitic phase transformation and the reverse transformation, respectively. C_R is the slope of the $\sigma_{crit}(T)$ curves for austenitic phase to R-phase transformation and R-phase to austenitic phase transformation. *Tr*: Room temperature, M_s: martensite transformation start temperature, A_s: reverse transformation start temperature, R_s: R-phase transformation start temperature, R_f: R-phase transformation finish temperature, R'_s: R-phase inverse transformation start temperature, R'_f: R-phase inverse transformation finish temperature.

The transformation tensor of martensite Ω^M and that of R-phase Ω^R were separated, respectively, into stress-induced and temperature-induced transformation tensors and symbolized as Ω_S^M, Ω_T^M, Ω_S^R and Ω_T^R. Since purely temperature-induced martensitic phase is generated only below the temperature of M_s, it is not necessary to consider Ω_T^M in this treatment. Then, the substitution of equations (6), (7) and (8) into equation (1) leads to the following equation.

$$\mathrm{d}\sigma = D\,\mathrm{d}\varepsilon + \Omega_S^M\,\mathrm{d}\xi_S^M + \Omega_S^R\,\mathrm{d}\xi_S^R + \Omega_T^R\,\mathrm{d}\xi_T^R + \Theta\,\mathrm{d}T. \tag{9}$$

If all material tensors are assumed to be constant, equation (9) is integrated as

$$\sigma - \sigma_0 = D(\varepsilon - \varepsilon_0) + \Omega_S^M\left(\xi_S^M - \xi_{S_0}^M\right) + \Omega_S^R\left(\xi_S^R - \xi_{S_0}^R\right) + \Omega_T^R\left(\xi_T^R - \xi_{T_0}^R\right) + \Theta(T - T_0). \tag{10}$$

Then, on the basis of the following three conditions, equations (11), (12) and (13) are derived.

(1) An SMA in 100% austenitic phase ($\sigma_0 = 0, \varepsilon_0 = 0, \xi_{S_0}^R = 0, \xi_{T_0}^R = 0, \xi_{S_0}^M = 0$) is loaded until it is transformed into 100% R-phase, and then unloaded ($\sigma = 0, \varepsilon = \varepsilon_L^R, \xi_S^R = 1, \xi_T^R = 0, \xi_S^M = 0$).

$$\Omega_S^R = -\varepsilon_L^R D. \tag{11}$$

(2) An SMA in 100% purely temperature-induced R-phase ($\sigma_0 = 0, \varepsilon_0 = 0, \xi_{S_0}^R = 0, \xi_{T_0}^R = 1, \xi_{S_0}^M = 0$) is loaded until it is transformed into 100% martensitic phase, and then unloaded ($\sigma = 0, \varepsilon = \varepsilon_L^M, \xi_S^R = 0, \xi_T^R = 0, \xi_S^M = 1$).

$$\Omega_S^M = -\varepsilon_L^M D. \tag{12}$$

(3) An SMA foil in 100% purely temperature-induced R-phase ($\sigma_0 = 0, \varepsilon_0 = 0, \xi_{S_0}^R = 0, \xi_{T_0}^R = 1, \xi_{S_0}^M = 0$) is loaded until it is transformed into 100% stress-induced R-phase, and then unloaded ($\sigma = 0, \varepsilon = \varepsilon_L^R, \xi_S^R = 1, \xi_T^R = 0, \xi_S^M = 0$).

$$\Omega_T^R = 0. \tag{13}$$

Moreover, in the same way as the equation (3), Θ is expressed by

$$\Theta = -\alpha D. \tag{14}$$

Next, the transformation tensors, Ω_S^M, Ω_S^R and Ω_T^R, and thermo-elastic tensor Θ are represented as functions of R-phase fraction ξ^R and martensitic phase fraction ξ^M: $\Omega_S^M(\xi^R, \xi_S^M)$, $\Omega_S^R(\xi_S^R, \xi^M)$, $\Omega_T^R(\xi_T^R, \xi^M)$ and $\Theta(\xi^R, \xi^M)$. On the assumption that elasticity tensor D and thermo-elasticity tensor α are the functions of ξ^R and ξ^M, they are described as

$$D(\xi^R, \xi^M) = D_A + \xi^R(D_R - D_A) + \xi^M(D_M - D_A), \tag{15}$$

$$\alpha(\xi^R, \xi^M) = \alpha_A + \xi^R(\alpha_R - \alpha_A) + \xi^M(\alpha_M - \alpha_A). \tag{16}$$

In an initial state, the following relations can be obtained from the equations (11), (12) and (14).

$$\Omega_S^R(\xi_{S_0}^R, \xi_0^M) = -\varepsilon_L^R D(\xi_0^R, \xi_0^M), \tag{17}$$

$$\Omega_S^M(\xi_0^R, \xi_{S_0}^M) = -\varepsilon_L^M D(\xi_0^R, \xi_{S_0}^M), \tag{18}$$

$$\Theta(\xi_0^R, \xi_0^M) = -\alpha(\xi_0^R, \xi_0^M) D(\xi_0^R, \xi_0^M). \tag{19}$$

Since D is a function of ξ^R and ξ^M, Ω_S^R, Ω_S^M and Θ are assumed to be also functions of the ξ^R and ξ^M. Then, Ω_S^R, Ω_S^M and Θ are expanded in Taylor series about ξ_0^R and ξ_0^M and higher order terms from second are neglected. By the substitution of equations from (15) to (19) into the Taylor series, the following relations can be obtained.

$$\Omega_S^R(\xi_S^R, \xi^M) = -\varepsilon_L^R D(\xi_S^R, \xi^M), \tag{20}$$

$$\Omega_S^M(\xi^R, \xi_S^M) = -\varepsilon_L^M D(\xi^R, \xi_S^M), \tag{21}$$

$$\Theta(\xi^R, \xi^M) = -\alpha(\xi^R, \xi^M) D(\xi^R, \xi^M). \tag{22}$$

On the other hand, since Ω_T^R is assumed to be constant independent of volume fraction ξ, it is extended from equation (13) as follows.

$$\Omega_T^R(\xi_T^R, \xi^M) \equiv 0. \tag{23}$$

Substituting equations (20), (21), (22) and (23) into (9), we can obtain the following relation.

$$\begin{aligned} \mathrm{d}\sigma = {} & D\left(\xi^R, \xi^M\right) \mathrm{d}\varepsilon - \varepsilon_L^M D\left(\xi^R, \xi^M\right) \mathrm{d}\xi_S^M - \varepsilon_L^R D\left(\xi^R, \xi^M\right) \mathrm{d}\xi_S^R \\ & - \alpha\left(\xi^R, \xi^M\right) D\left(\xi^R, \xi^M\right) \mathrm{d}T. \end{aligned} \tag{24}$$

Since the stress-induced fractions are the functions of stress and temperature, ξ_S^R and ξ_S^M are expressed as

$$\mathrm{d}\xi_S^R = \frac{\partial \xi_S^R}{\partial \sigma} \mathrm{d}\sigma + \frac{\partial \xi_S^R}{\partial T} \mathrm{d}T, \tag{25}$$

$$\mathrm{d}\xi_S^M = \frac{\partial \xi_S^M}{\partial \sigma} \mathrm{d}\sigma + \frac{\partial \xi_S^M}{\partial T} \mathrm{d}T. \tag{26}$$

From the equations (24) to (26), the constitutive equation of this model is obtained as

$$\begin{aligned} \mathrm{d}\sigma = {} & \frac{1}{1 + \varepsilon_L^R D(\xi^R, \xi^M) \dfrac{\partial \xi_S^R}{\partial \sigma} + \varepsilon_L^M D(\xi^R, \xi^M) \dfrac{\partial \xi_S^M}{\partial \sigma}} \\ & \times \left[D\left(\xi^R, \xi^M\right) \mathrm{d}\varepsilon - \left\{ \varepsilon_L^R D\left(\xi^R, \xi^M\right) \frac{\partial \xi_S^R}{\partial T} + \varepsilon_L^M D\left(\xi^R, \xi^M\right) \frac{\partial \xi_S^M}{\partial T} \right. \right. \\ & \left. \left. + \alpha\left(\xi^R, \xi^M\right) D\left(\xi^R, \xi^M\right) \right\} \mathrm{d}T \right]. \end{aligned} \tag{27}$$

Finally, stress-induced martensite fraction and stress-induced R-phase fraction are assumed to be represented using cosine functions, following Liang and Rogers [4]. On the basis of Fig. 3, the fractions are described as equations from (28) to (32). In these equations, σ_M^{band} and σ_A^{band} are the widths of the martensite transformation and the reverse transformation along the vertical axis in Fig. 3; σ_R^{min} and σ_R^{max} are the critical stress of R-phase accommodation start and that of its finish. R_s' and R_f' are equal to R_f and R_s in this model.

(1) Martensite transformation

$$\xi_S^M = \frac{1 - \xi_{S_0}^M}{2} \cos \frac{\pi}{\sigma_M^{band}} \left\{ \sigma - \sigma_M^{band} - C_M (T - M_s) \right\} + \frac{1 + \xi_{S_0}^M}{2}. \tag{28}$$

(2) Reverse transformation

$$\xi_S^M = \frac{\xi_{S_0}^M}{2} \left[\cos \frac{\pi}{\sigma_A^{band}} \left\{ \sigma - C_A (T - A_s) \right\} + 1 \right]. \tag{29}$$

(3) R-phase transformation

$$\xi_S^R = \frac{1 - \xi_{S_0}^R}{2} \cos \frac{\pi}{C_R (R_s - R_f)} \left\{ \sigma - C_R (T - R_f) \right\} + \frac{1 + \xi_{S_0}^R}{2}. \tag{30}$$

(4) R-phase inverse transformation

$$\xi_S^R = \frac{\xi_{S_0}^R}{2}\left[\cos\frac{\pi}{C_R(R'_f - R'_s)}\{\sigma - C_R(T - R'_s)\} + 1\right]. \tag{31}$$

(5) R-phase accommodation

$$\xi_S^R = \frac{1 - \xi_{S_0}^R}{2}\cos\left\{\frac{\pi}{\sigma_R^{max} - \sigma_R^{min}}(\sigma - \sigma_R^{max})\right\} + \frac{1 + \xi_{S_0}^M}{2}. \tag{32}$$

3. EXPERIMENTS TO DETERMINE THE PARAMETERS OF THE CONSTITUTIVE EQUATION

In order to obtain the mechanical properties of the SMA foil and to determine the parameters of the constitutive equation derived in the previous section, experimental tests were carried out for the SMA foils.

The SMA foils used in this research were Ti-50.2%Ni foils (Furukawa Electric Co. Ltd.) of thickness 0.045 mm. For the improvement of the adhesion performance to the resin of CFRP laminates, the surface of the foils was treated with 10% NaOH anode oxidation [8]. Dimensions of specimens were: length = 120 mm, width = 20 mm, thickness = 0.045 mm, and gauge length = 60 mm.

3.1. Tensile loading–unloading tests

Tensile loading–unloading tests were carried out to obtain stress–strain curves at various temperatures. These specimens were loaded at the cross-head speed of 0.5 mm/min until the martensite transformation was complete. When the martensite transformation started, the load became constant. After the transformation finished, the load increased elastically again. After that, the specimens were unloaded. Figures 4 and 5 show the stress–strain curves of the SMA foil at 25°C and 90°C, respectively.

On the basis of the stress–strain curves, parameters of the consititutive equation (ε_L^M, ε_L^R, σ_R^{max} and σ_R^{min}) and Young's moduli (E_{SIR}, E_{SAR}, E_M and E_A) were determined as shown in Figs 4 and 5. In this research, SMA was assumed to consist of purely temperature-induced R-phase before loading at 25°C. This phase is called the self-accommodation rhombohedral (SAR), and appears while the temperature falls. On the other hand, stress-induced R-phase is called the stress-induced rhombohedral (SIR). In Fig. 4, it was observed that R-phase transformation occurred at lower strain level than the martensite transformation.

Figure 6 shows the martensite transformation region at various temperatures. The start and finish critical stresses were measured by the tensite tests. The parameters of the constitutive model (M_s, C_M, σ_M^{band} and σ_A^{band}) were determined as shown in Fig. 6.

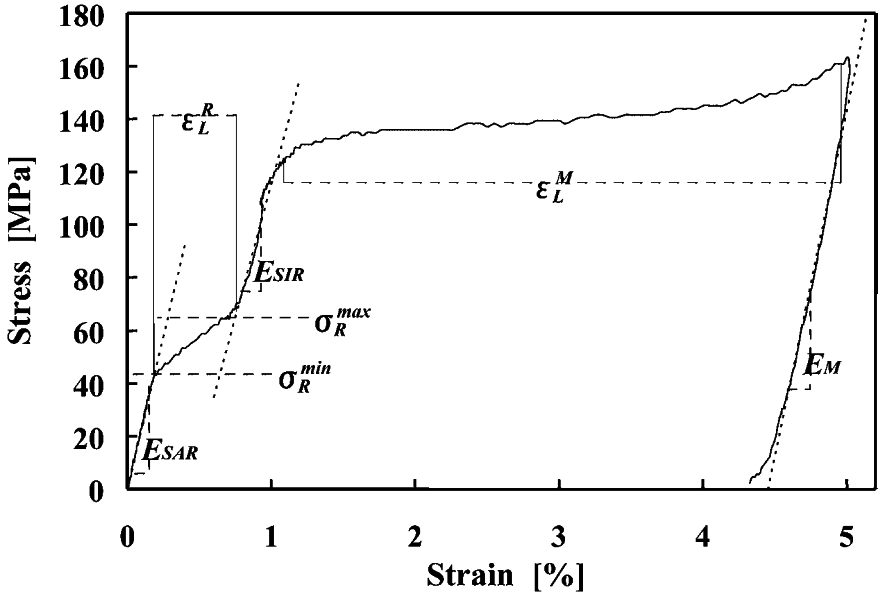

Figure 4. Stress–strain curve of the SMA foil at 25°C obtained from loading—unloading test. ε_L^R, ε_L^M, E_{SAR}, E_{SIR}, E_M, σ_R^{max} and σ_R^{min} were determined from this curve.

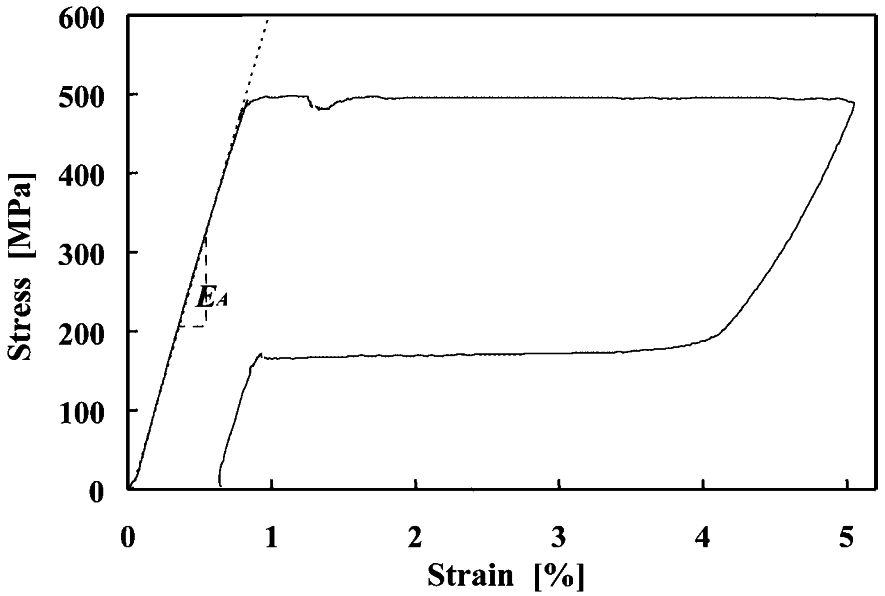

Figure 5. Stress–strain curve of the SMA foil at 90°C obtained from loading–unloading test in the thermostatic chamber. E_A was determined from this curve.

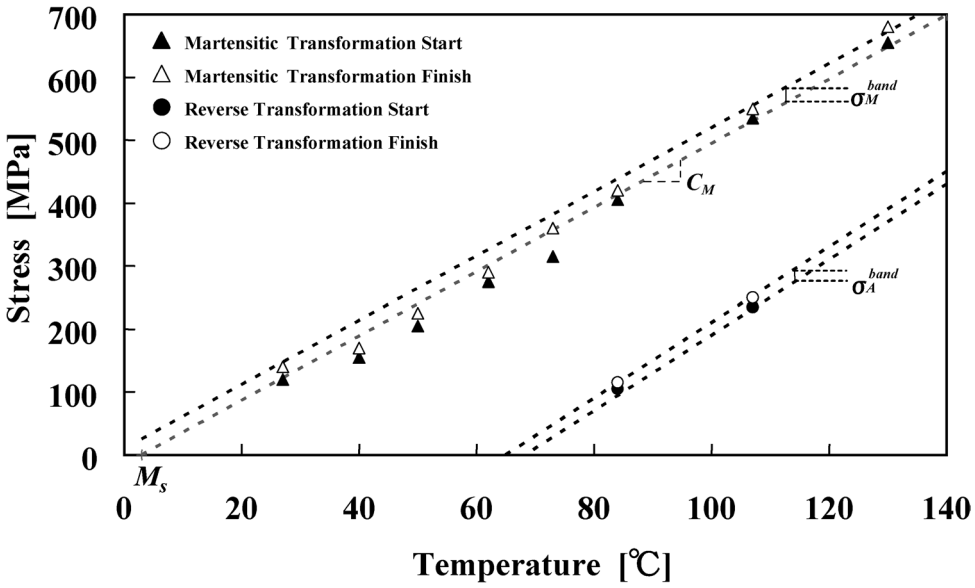

Figure 6. Critical stresses *versus* temperature representing transformations of Ti-Ni SMA, obtained from the experimental tests. The martensite transformation region σ_M^{band}, the reverse transformation region σ_A^{band}, the slope C_M, and martensite transformation start temperature M_S were obtained from these results.

3.2. Heating tests with a thermostatic chamber

First, the specimens were loaded to introduce various levels of residual strain at 25°C. Then both ends of the specimens were fixed to keep their length. Through the heating of the specimens in a thermostatic chamber, their recovery stresses were measured at various temperatures. Figure 7 shows the dependence of the recovery stress on temperature. C_A was determined from the slope of the recovery stress.

Table 1 summarizes the properties of SMA foils determined from the experimental results. However R_s, R_f, A_s and C_R could not be measured experimentally. Thus, R_s, R_f and A_s were quoted from the reference [9], in which these values were measured with a differential scanning calorimeter, and C_R was determined from the reference [10].

4. SIMULATION OF THE BEHAVIOR OF SMA

The behavior of the SMA foil was theoretically calculated using the newly derived constitutive equation. In this calculation, SMA foil was loaded up to the predetermined strain level from 0.5% to 7.0%, then unloaded.

Figures 8 and 9 show the calculated stress−strain curves at 25°C and 90°C, respectively. In Figs 10 and 11, experimental results in Figs 4 and 5 and calculated results in Figs 8 and 9 were compared, respectively. Figure 10 indicates that the calculated results well reproduced the stress–strain curves at 25°C. On the other

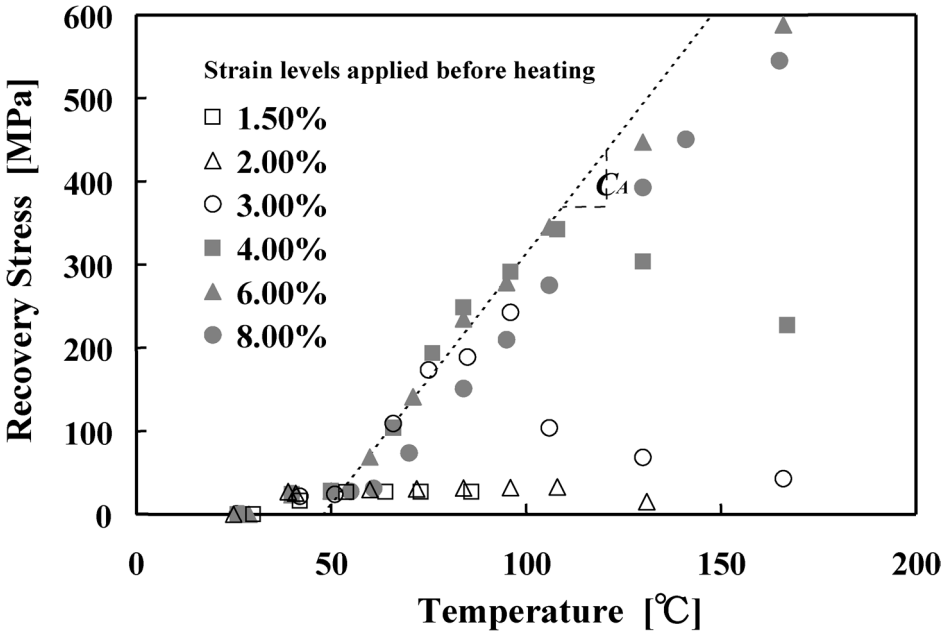

Figure 7. Recovery stress of SMA foils *versus* temperature. The slope C_A was determined from these results.

Table 1.
Properties of SMA foil which were determined from the experimental results

Young's moduli (GPa)		Stress (MPa)		Strain (%)		Transition temperatures (°C)		Gradients (MPa/°C)	
E_{SAR}	23	σ_M^{band}	25	ε_L^M	5	M_s	3	C_M	5.1
E_{SIR}	23	σ_R^{max}	62	ε_L^R	0.6	R_s^*	49.7	C_R^*	18
E_M	26	σ_R^{min}	40			R_f^*	38.3	C_A	6
E_A	63	σ_A^{band}	20			A_s^*	47.9		

SAR: self-accomodation rhombohedral, *SIR*: self-induced rhombohedral; σ_M^{band}: martensite transformation region, σ_A^{band}: reverse transformation region; σ_R^{min} and σ_R^{max} are the critical stress of R-phase accommodation start and that of its finish, respectively; M_s: martensite transformation start temperature, R_s: R-phase transformation start temperature, R_f: R-phase transformation finish temperature, A_s: reverse transformation start temperature; C_M and C_A are the slopes of the $\sigma crit(T)$ curves for the austenitic phase to martensitic phase transformation and the reverse transformation, respectively; $C_R$is the slope of the $\sigma crit(T)$ curves for austenitic phase to R-phase transformation and R-phase to austenitic phase transformation.

*R_s, R_f and A_s were quoted from the reference [9], and C_R from the Ref. [10].

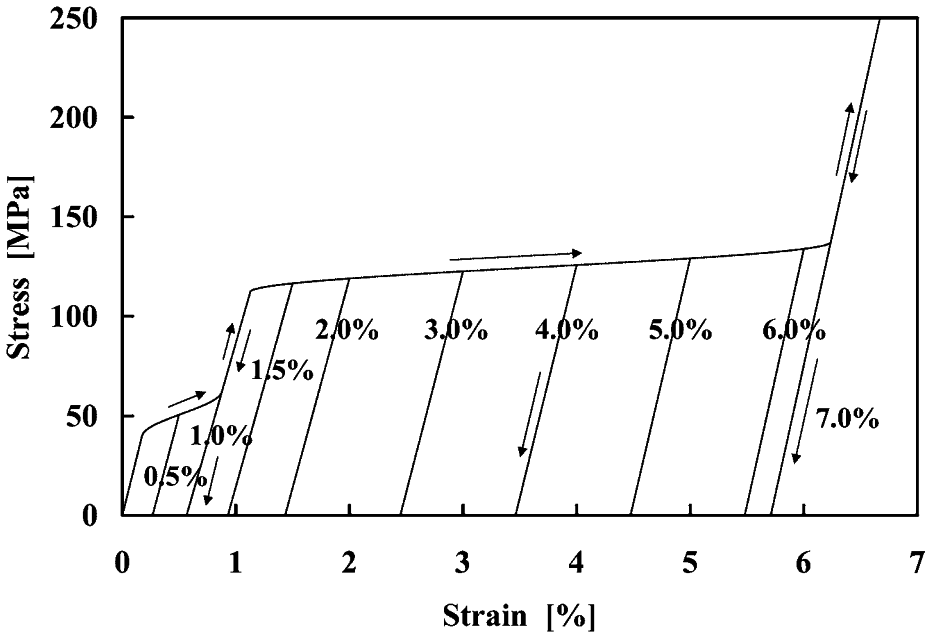

Figure 8. Calculated stress–strain curves of SMA at 25°C, which illustrate the residual strains after various levels of tensile strain are applied.

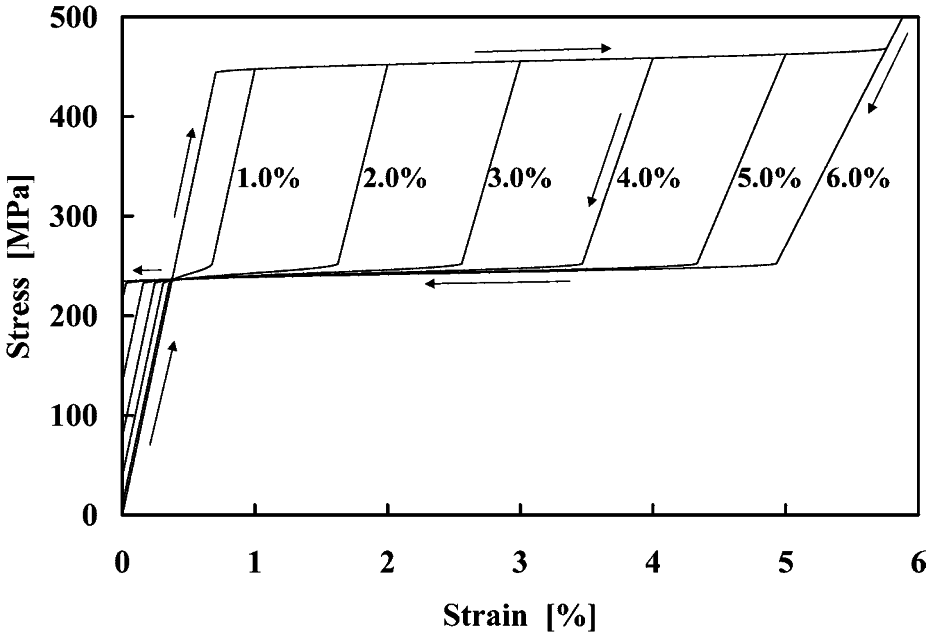

Figure 9. Calculated stress–strain curves of SMA at 90°C, which illustrate the pseudo-elasticity.

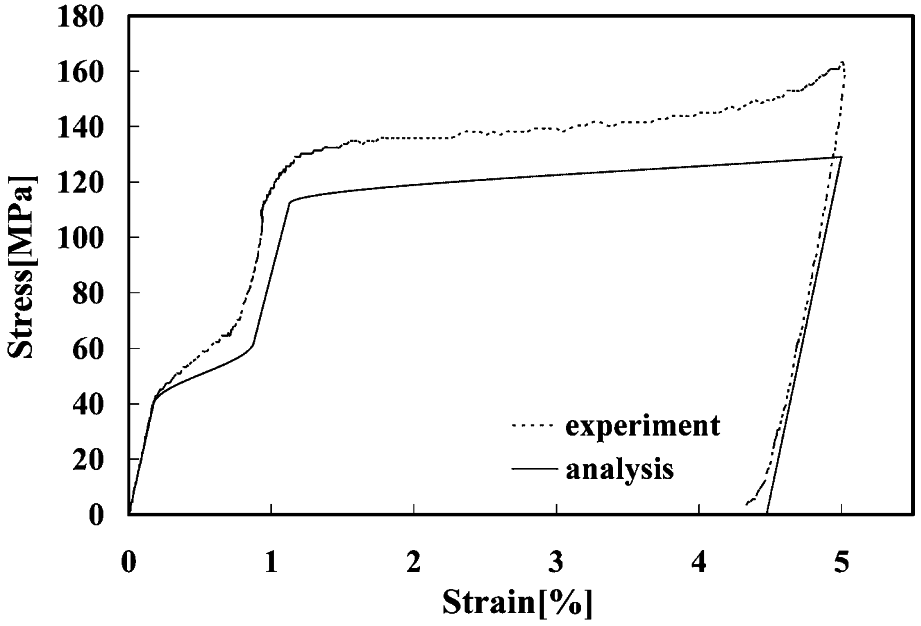

Figure 10. Comparison between experimental and calculated stress–strain curves of SMA at 25°C.

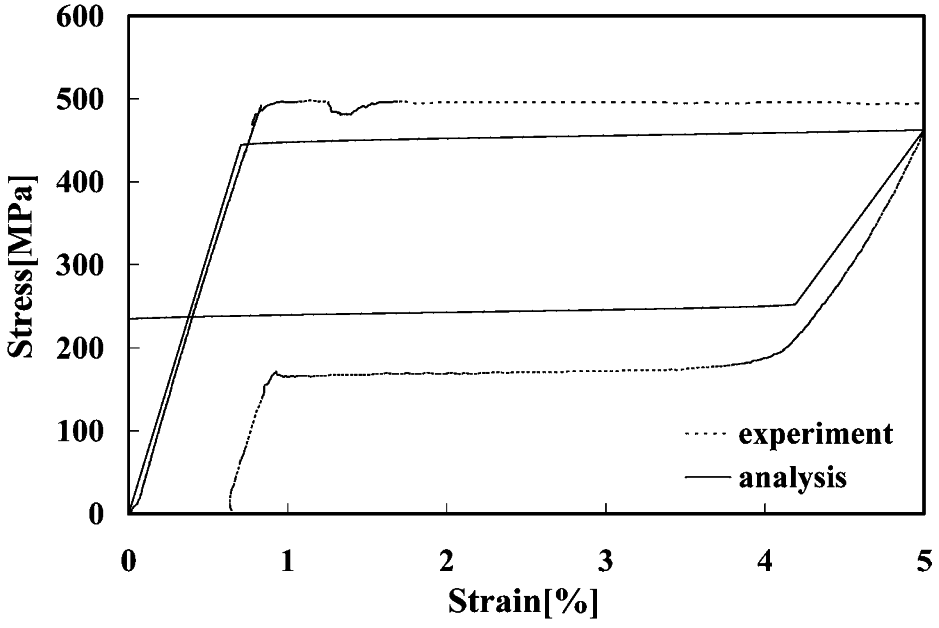

Figure 11. Comparison between experimental and calculated stress–strain curves of SMA at 90°C.

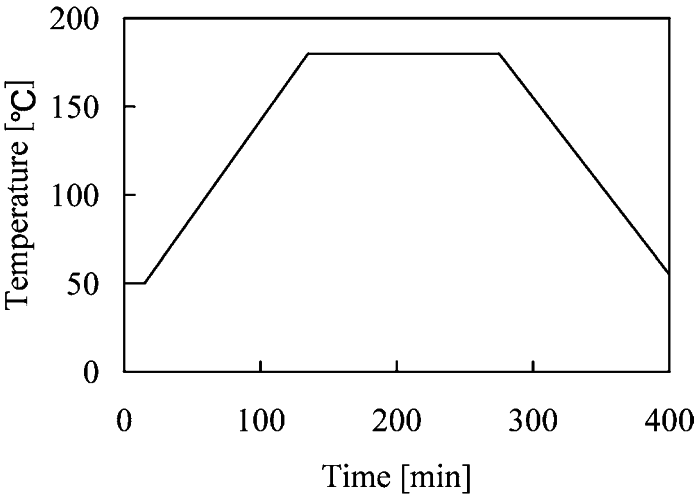

Figure 12. Temperature profile in the manufacturing process of the CFRP laminate (T300/F593, Hexcel Co. Ltd.).

hand, compared with the experimental result at 90°C, the SMA shrinks excessively after unloading in the calculated result as shown in Fig. 11. This is because the compressive strain in the reverse transformation is assumed to be equivalent to the tensile strain required for the martensite transformation in this analysis. However, the calculation results have the similar tendency in the stress–strain curves. These agreements show that the newly extended Brinson model considering the R-phase is highly effective in representing the behavior of Ti-Ni SMA alloy.

Finally, in order to consider the embedment of the SMA into a CFRP laminate, the recovery stress profile of a 4% pre-strained SMA foil during the manufacturing process of the CFRP laminate was calculated using this model. The temperature profile of the manufacturing process is shown in Fig. 12. Both ends of the SMA foil were fixed to prevent shrinkage, and heated along the temperature profile. After the manufacturing process, the SMA foil was heated again to 90°C. The calculated result is shown in Fig. 13. This result indicates that the recovery stress remains at the room temperature of 25°C after the manufacturing. This fact suggests that the recovery stress depends on the temperature history.

Furthermore, stress–strain curves of the 4% pre-strained SMA foil at 25°C and 90°C were calculated following the simulation of the manufacturing process, as shown in Figs 14 and 15, respectively. These results clarified that the recovery stress already existed before loading and indicated that the occurrence of transverse cracks might be suppressed by the residual recovery stress.

5. CONCLUSIONS

In this research, the authors have proposed an extended Brinson model to represent the specific characteristics of Ti-Ni SMA foil considering R-phase and derived a

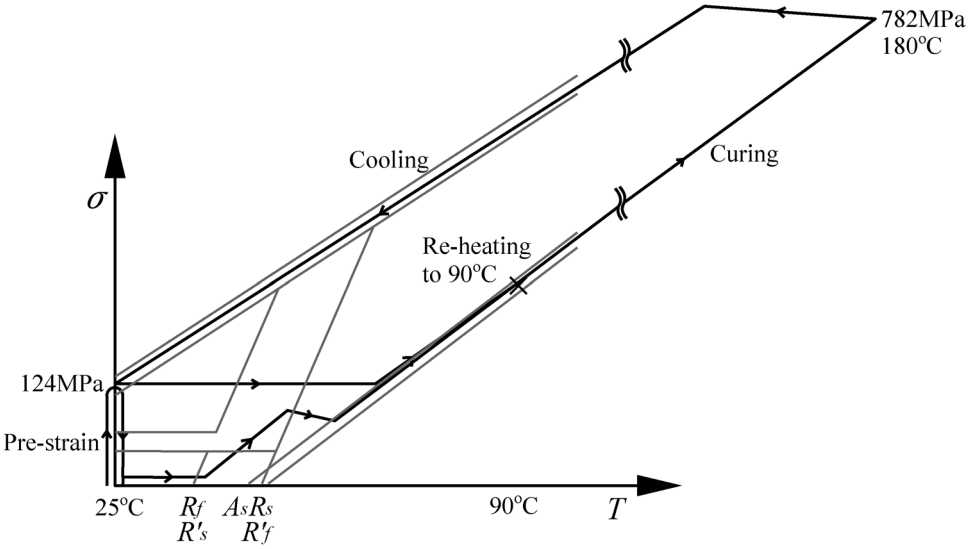

Figure 13. Recovery stress of an SMA foil during the manufacturing process of a CFRP laminate, in which a 4% pre-strained SMA foil was embedded.

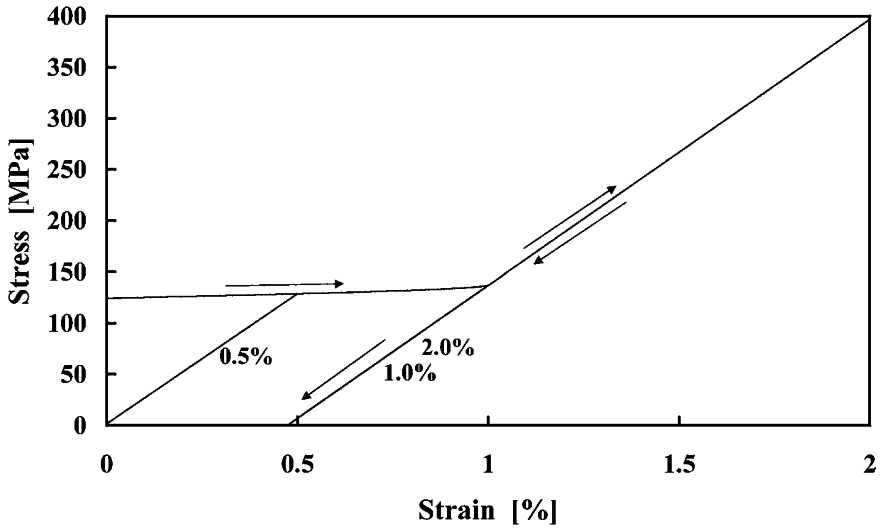

Figure 14. Calculated stress–strain curves of the 4% pre-strained SMA embedded in a CFRP laminate at 25°C. The laminate was loaded up to the predetermined strain levels of 0.5%, 1.0% and 2.0% at 25°C.

constitutive equation that comprehensively described the stress–strain relation of the SMA foil in both loading and unloading process. Since the calculated stress–strain curves at 25°C and 90°C corresponded with experimental ones, this model was shown to be adequate. Moreover, considering that 4% pre-strained SMA foil was embedded into CFRP cross-ply laminate, the behavior of the SMA foil during the

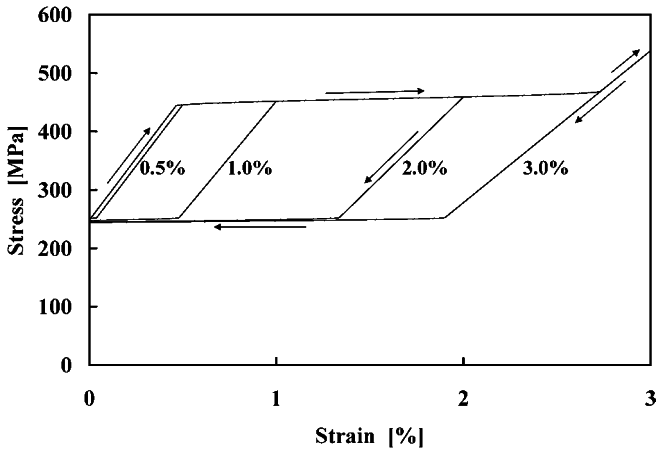

Figure 15. Calculated stress–strain curves of 4% pre-strained SMA embedded in a CFRP laminate at 90°C. The laminate was loaded up to the predetermined strain levels of 0.5%, 1.0% and 2.0% at 90°C.

CFRP manufacturing process was calculated theoretically. The calculations proved that the recovery stress already existed in the laminate after the manufacturing process. Thus the occurrence of transverse cracks might be suppressed with the embedment of 4% pre-strained SMA into CFRP cross-ply laminate.

The authors clarified experimentally that 4% pre-strained SMA foil suppressed not only the occurrence but also the progress of transverse cracks in CFRP laminate, which was represented in our previous article [2]. This research theoretically confirmed that the embedment of 4% pre-strained SMA foil was effective in suppressing the occurrence of transverse cracking. In the following paper, we will prove theoretically the fact that the progress of transverse cracks is also suppressed, using the constitutive equation proposed in this research.

REFERENCES

1. S. Ogihara, S. Kobayashi and N. Takeda, Effect of embedded SMA fibers on the damage progress in composite laminate, *J. Mater. Sci. Lett.* **20**, 1139–1141 (2001).
2. I. Taketa, M. Amano, Y. Okabe and N. Takeda, Damage detection and suppression system of CFRP laminates with FBG sensor and SMA actuator, *Trans. MRS-J* **28** (1/4), 675–678 (2003).
3. K. Tanaka, A thermo-mechanical sketch of shape memory effect: one-dimensional tensile behavior, *Res. Mech.* **18** (3), 251–263 (2002).
4. C. Liang and C. A. Rogers, A one-dimensional thermomechanical constitutive relation of shape memory materials, *J. Intel. Mater. Syst. Struct.* **1** (2), 207–234 (1990).
5. L. C. Brinson, One-dimensional constitutive behavior of shape memory alloys: thermomechanical derivation with non-constant material functions and redefined martensite internal variable, *J. Intel. Mat. Syst. Struct.* **4** (2), 229–242 (1993).
6. S. Miyazaki and K. Otsuka, Deformation and transition behavior associated with the R-phase in Ti-Ni alloys, *Metall. Trans. A* **17** (1), 53–63 (1986).

7. T. Kamita and Y. Matsuzaki, One-dimensional pseudoelastic theory of shape memory alloys, *Smart Mater. Struct.* **7**, 489–495 (1998).
8. T. Ogisu, N. Ando, J. Takaki, T. Okabe and N. Takeda, Improved surface treatment of SMA foils and damage suppression of SMA-foil embedded CFRP laminates, *J. Intel. Mater. Syst. Struct.* **12** (4), 265–270 (2001).
9. M. Kobayashi, Effect of microscopic-damage suppression in CFRP laminates with embedded SMA foils, Master Thesis, Univ. of Tokyo (2000) (in Japanese).
10. H. Tobushi, K. Tanaka, K. Kimura, T. Hori and T. Sawada, Stress-strain-temperature relation associated with the R-phase transformation in TiNi shape memory alloy, *Trans. JSME* **57** (543), 2753–2759 (1991) (in Japanese).